Available online at www.sciencedirect.com

ScienceDirect

Additive Manufacturing 1–4 (2014) 52–63

Additive MANUFACTURING

www.elsevier.com/locate/addma

Toward an integrated computational system for describing the additive manufacturing process for metallic materials☆,☆☆

Richard Martukanitz[a,b,*], Pan Michaleris[a,c,d], Todd Palmer[a,b,e], Tarasankar DebRoy[a,e], Zi-Kui Liu[a,e], Richard Otis[e], Tae Wook Heo[e], Long-Qing Chen[a,e]

[a] *Center for Innovative Materials Processing through Direct Digital Deposition, Pennsylvania State University, State College, PA 16801, United States*
[b] *Applied Research Laboratory, Pennsylvania State University, State College, PA 16801, United States*
[c] *Mechanical and Nuclear Engineering Department, Pennsylvania State University, State College, PA 16802, United States*
[d] *Pan Computing LLC, State College, PA 16801, United States*
[e] *Material Science and Engineering Department, Pennsylvania State University, State College, PA 16802, United States*

Received 12 May 2014; received in revised form 8 August 2014; accepted 10 September 2014
Available online 19 September 2014

Abstract

The ability to simulate the thermal, mechanical, and material response in additive manufacturing offers tremendous utility for gaining a deeper understanding of the process, while also having significant practical application. The approach and progress in establishing an integrated computational system for simulating additive manufacturing of metallic components are discussed, with the primary focus directed at the computational intensive components, which include the process and material models. The ability to experimentally measure key characteristics for verification of the models is also presented and is seen as critical in the development of the integrated computational system. Two examples are also presented that utilize the current features of the analyses techniques for exploring and applying additive manufacturing technology.

Keywords: Additive manufacturing; Metallic materials; Process; Materials; Modeling

1. Introduction

Additive manufacturing (AM) for metallic materials represents a group of novel, formative, manufacturing processes by which functional components are produced directly from a digital part description. In contrast to conventional formative (joining) and subtractive (machining) processes, metallic components or structures are manufactured in a sequential manner through a layer-wise addition of material, in the case of the directed energy process, or selective consolidation of preplaced powder, such as with the powder bed fusion process. Components produced using these processes may comprise volumes of material ranging from approximately 1 cm^3 to greater than 1 m^3. The interaction of the material, energy source, motion system, sensors, and controls that govern AM processes represents a broad range of engineering and scientific principles. Frazier has recently provided an excellent review of the subject [1].

The ability to simulate the various functions that comprise the additive manufacturing process within an integrated computational system offers tremendous opportunities for optimizing processing conditions, ensuring material quality, ensuring dimensional attributes, developing initial process metrics, and accelerating process acceptance. In the case of producing functional components in metallic materials through additive manufacturing, consideration must be given to not only form and fit, but also function. In many instances, the functionality of the part will be governed by its mechanical properties, which in turn are closely defined by the process and resultant

☆ One or more authors of this article are part of the Editorial Board of the journal. Full responsibility for the editorial and peer-review process for this article lies with the journal's Editor-in-Chief Prof. Ryan Wicker and Deputy Editor Prof. Eric MacDonald. Furthermore, the authors of this article had no and do not currently have access to any confidential information related to its peer-review process.

☆☆ Submitted to the Inaugural Edition of Additive Manufacturing, Elsevier, June, 2014.

* Corresponding author at: Center for Innovative Materials Processing through Direct Digital Deposition, Pennsylvania State University, State College, PA 16801, United States. Tel.: +1 814 863 7282; fax: +1 814 865 0865.
E-mail addresses: rxm44@arl.psu.edu, rxm44@psu.edu (R. Martukanitz).

http://dx.doi.org/10.1016/j.addma.2014.09.002
2214-8604/

microstructures. Another important aspect that has broad implications is the generation of residual stress states and the ensuing thermal distortion generated during the process. The ability to describe these conditions are typically defined within general computational methods involving the physical description of the process in terms of energy and mass transport, followed by the ensuing effect on microstructural development, and finally, mechanical properties anticipated from the resultant microstructure. Although this methodology typically follows the general "process-microstructure-property" approach, the application of these principles to additive manufacturing poses several challenges. Firstly, the numerical simulation must accurately mimic the physical process. Secondly, it must capture sufficient detail of the process to enable meaningful predictive capabilities, and finally the simulation must be capable of representing a highly dynamic process.

Additive manufacturing processes for metallic materials representing actual components involves relative complex motion between the heat source and the substrate to produce the various layers that will eventually constitute the final part. The digital process that is used to accomplish this begins with a CAD model that is translated into an STL (Standard Tessellation Language) file format, which defines the exterior of the three-dimensional part through normal vectors of a triangulated surface. The STL file is then utilized to create a slice file of the part that drives the motion of the additive manufacturing system to produce two-dimensional layers necessary for creating the part geometry. The specific motion used to produce the individual layers may be external or internal to the additive manufacturing machine.

The motion required to produce an individual layer is usually complex, involving a wide range of velocities over a two-dimensional plane. Although current numerical schemes, such as finite element or finite difference, are easily capable of representing this motion, the necessity to accurately depict the convoluted movement of the heat source directly influences the location and size of the elements within the computational domain, as well as the modification of the grid during subsequent layers. This entire process has direct consequences on the computational efficiency of the model. Simple, single track models that allow the computational grid to be relatively straightforward are not considered in this framework, since the technique does not provide ample representation for most applications.

Both laser-based powder bed fusion and directed energy deposition processes utilize fiber delivered lasers, and the inherent nature of fiber delivery is the creation of the focused beam having a "top hat" energy distribution, shown in Fig. 1, with the diameter being related to the fiber diameter and the degree of focus at the substrate [2]. Lasers employed for powder bed fusion are relatively low power, in the range of 200–400 W, and utilize smaller fiber diameters that result in a spot size of between 50 and 100 μm. Lasers used for directed energy deposition may range between 500 and 10 kW, and are normally used with a defocused beam having a diameter of 300–3000 μm.

Electron beams used for directed energy deposition and powder bed fusion display more of a Gaussian distribution, with the "sharpness" of the beam being controlled by the accelerating voltage, beam current, and the focus coil current setting [3]. The

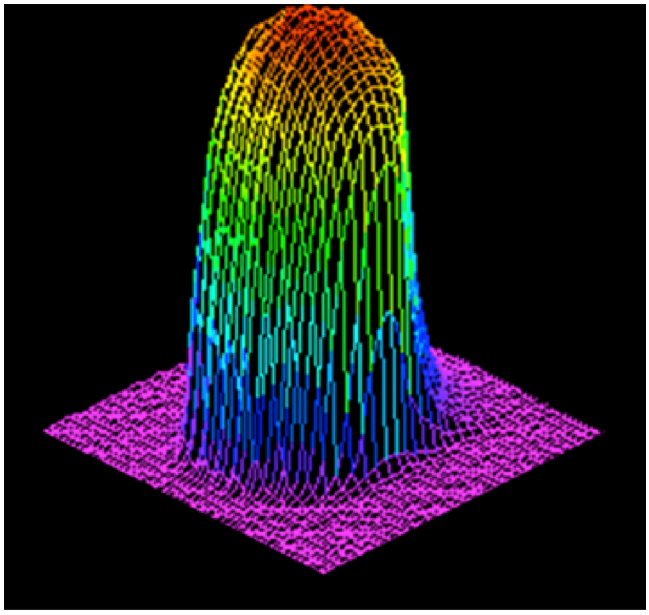

Fig. 1. Measured three-dimensional representation of a top hat energy distribution for a multi-kilowatt ytterbium fiber laser used for directed energy deposition.

electron beam may also be defocused, as well as rapidly manipulated using electromagnetic coils to achieve a more diffuse heat source. The power of the electron beam employed for powder bed fusion is around 3 kW, and electron beam power used for directed energy deposition may be anywhere from 2 to 20 kW.

Although both categories of additive manufacturing of metals involve the repetitive creation of layers through melting and solidification of material, there are major distinctions between the two processes which have ramifications to the physical models that may be used to describe these processes. The directed energy deposition process involves a lower velocity movement at higher power where the added material is either powder that is provided coaxially to a laser beam or wire directed into the interaction region between the electron beam and the substrate. Heating and melting simultaneously occur within the feedstock and the substrate beneath the beam. Exchange of energy encompasses the direct transfer between the energy source and the material, as well as mass and energy transport. In the case of powder bed fusion techniques, a lower power laser or electron beam is rapidly scanned over a pre-deposited powder layer to melt and solidify the surface. The exchange of energy for laser beam processing is the interaction of photons with electrons within the material; whereas, the transfer of energy for electron beam processing is governed by the kinetic energy of the accelerating electrons being transformed to heat upon collision with the material. Fig. 2 illustrates the directed energy and powder bed fusion processes for a top hat energy distribution and the formation of a single layer.

Although Fig. 2 depicts a "quasi steady state" condition for simplicity, the actual response of the material is highly dynamic. As the heat source moves relative to the substrate, the thermal fields generated within the material follow the heat source and change continually. For the underlying material near the path of the heat source, this results in rapid heating, and melting

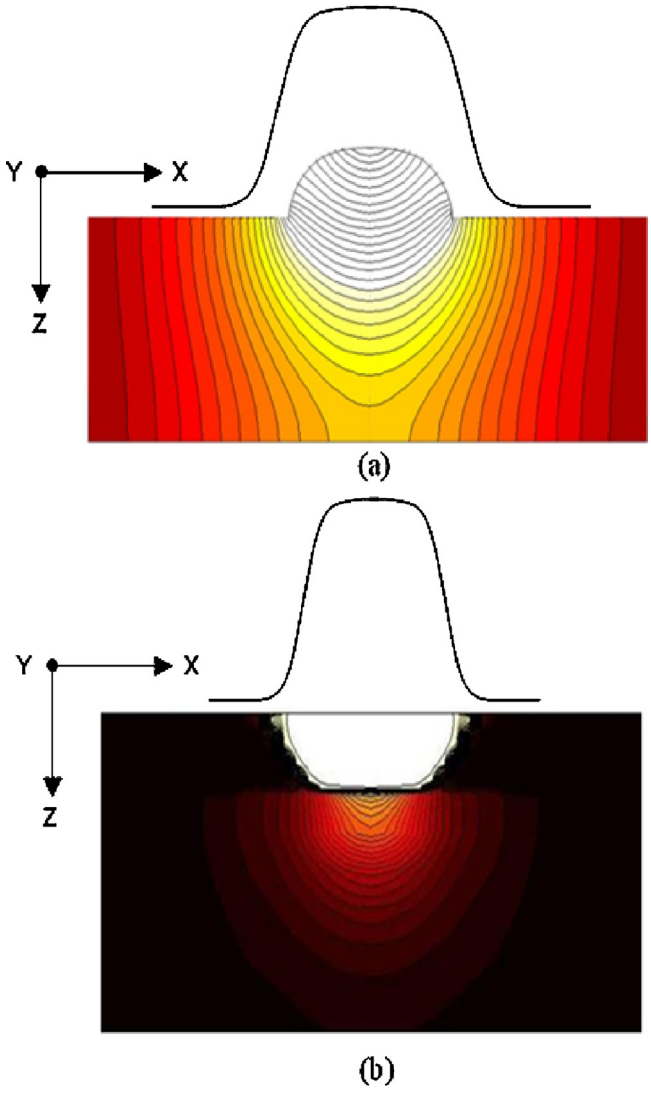

Fig. 2. Schematic of additive manufacturing describing the (a) directed energy deposition process and (b) powder bed fusion process.

directly below the heat source, followed by rapid cooling. Temperatures directly beneath the heat source will also result in some degree of evaporation of the liquid, and preferential evaporation will occur for high vapor pressure species within an alloy. Shown in Fig. 3 are measured temperatures over time using fine tungsten-rhenium thermocouples embedded on the top surface at the center plane of an Inconel 625^{TM} substrate after depositing 5 layers of Inconel 625^{TM} material using the laser-based directed energy deposition process. The process was conducted on a plate having dimensions of 12.5 mm by 76 mm by 152 mm with an absorbed laser power measured to be 660 W, a scan velocity of 1.0 cm/s, and a powder mass flow rate of 0.12 g/s fed coaxially with the beam [4].

As mentioned earlier, the materials response to the repetitive thermal transients occurring during additive manufacturing is dynamic and complex. The flow of heat is governed by conductions and surface heat losses, which are dependent upon the location within the build. For directed energy deposition, conduction typically dominates the early stages of the process when the build layers are in close proximity to the starting plate. However, as the deposition height rises and the underlying substrate temperature increases, surface conduction and radiation also play an important role in extracting heat, except for the electron beam process, which is performed within a vacuum and relies solely on radiation at the surface. During the initial stages of the build, these conditions result in directional solidification, which begins within the underlying substrate and progresses to the current deposit [5,6]. The direction of solidification is opposite the primary direction of heat flow and in the direction of the build. The directional solidification is also encouraged by epitaxy between the partially remelted substrate and the liquid deposit that continues the crystallographic orientation in the easy growth direction. For powder bed fusion techniques, the insulating quality of the surrounding, unfused powder somewhat lessens the effect of directional heat flow; however, epitaxial growth remains operative for many alloys [7,8].

Fig. 4 illustrates the macro and micro-structures observed in a directed energy deposition process for Ti–6Al–4V alloy in the as-built condition. The macrostructure, to the left in the figure, depicts the multiple passes used to produce the feature, as well as large columnar β-phase grains growing in the direction of the build. Although the grain directionality is less distinguishable in the observed microstructures, which is primarily due to the transformation of β to α and α' phases after solidification, the directional growth is slightly discernible within the microstructures through faint prior β grain boundaries. The microstructural anisotropy that is found during additive manufacturing of many alloys also manifests itself as mechanical property anisotropy or change in strength and other characteristics based on the orientation within the build [1,9,10].

2. Integrated computational approach

Aspects of the additive manufacturing processes that are considered for computational simulations include the thermal and mechanical response of the material during and after processing, the evolution of the material's microstructure during processing, and the mechanical properties representing the material that result from the development of the final microstructure. There is significant utility in linking these analyses within an integrated framework that provides an accurate depiction of the part geometry and build sequence, manages the multiple spatial scales that are involved, and allows the sequential flow of data between functions. Shown in Fig. 5 is the integrated computational system for describing additive manufacturing of metallic systems under development at the Center for Innovative Material Processing through Direct Digital Deposition (CIMP-3D) at the Pennsylvania State University. The creation of this system involves a wide range of individuals having significant expertise in computational analysis, as well as in obtaining experimental information that may be utilized for validation.

As illustrated in Fig. 5, the integrated computational system under development entails various analysis methods required to obtain critical information concerning additive manufacturing of metallic materials in a virtual environment. The components of the system that are computationally intensive include the

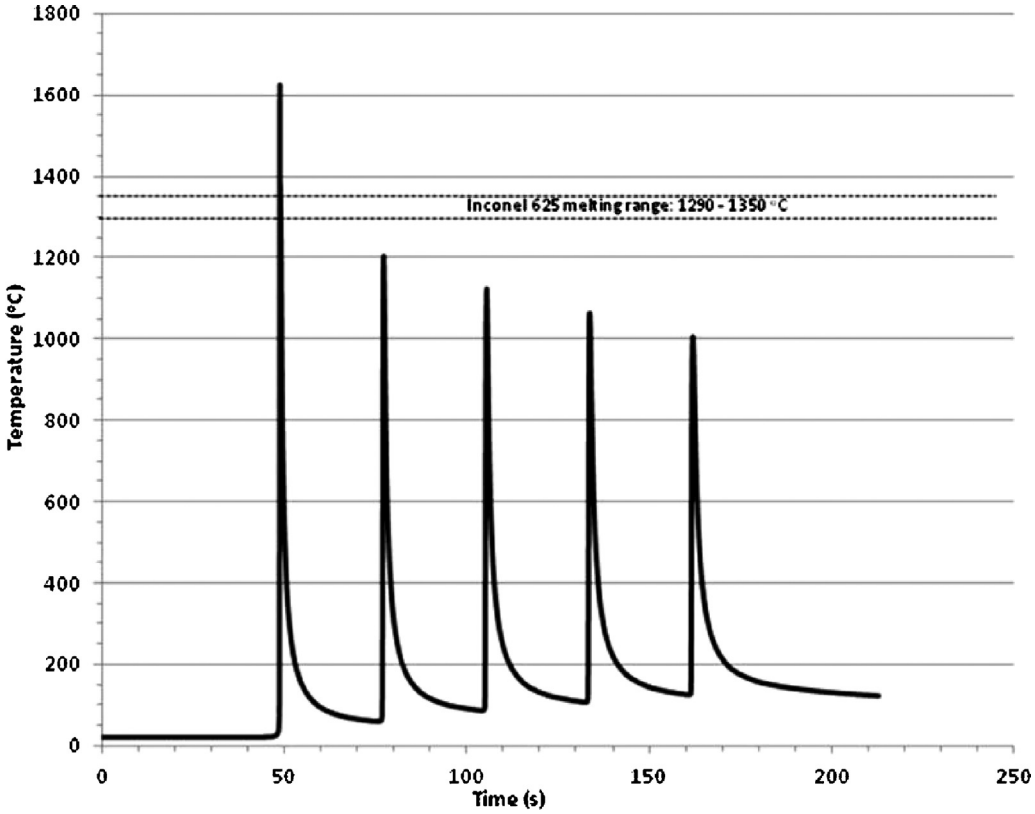

Fig. 3. Detailed measurements of temperature over time at the surface of an Inconel 625™ substrate directly under an Inconel 625™ deposit representing five passes produced using the directed laser deposition process.

simulation of the material's thermal and mechanical response to the process (thermo-mechanical simulations) and the evolution of the material's microstructure based on the thermal excursions representing the process. Since thermo-mechanical and microstructural analyses are seen as critical for obtaining important information regarding the additive manufacturing process and are the most computationally intensive components, these subjects will be the primary focus of this discussion.

It should be noted that although the various analyses are integrated within the engineering system, the computation is uncoupled between functions. The obvious advantage of an uncoupled formulation at this stage is the ability of the modules to be independently developed assuming that a data exchange format, that includes appropriate units and scaling, is utilized. The greatest challenge in data transfer lies in simulating the motion of the heat source based on the machine or software build plan. The simulation for thermal and mechanical response of the material, representing the process model, must truly mimic the actual build sequence, and this requires considerable coordination between the path plan, generation of the computational grid, and motion of the heat source within the model.

Data requirements for the integrated computational system begin with the STL file describing surfaces of the part to be built. Based on the STL file input, the slicing procedure generated by the additive manufacturing system, when available, is transposed using a custom translator to generate the layer geometries and motion of the heat source within a Cartesian system. The use of the custom translator enables the computational grid for thermo-mechanical simulations to be created automatically; however, when the slicing arrangement is not easily transferable from the machine, manual creation of the geometry and path plans are required. The output file of the thermo-mechanical simulation is time, temperature, displacement, and stress for each computational node/element within the model. The TTSP (time, temperature, and stress at position) file represents formatted text that may be used as input for microstructural simulations for positions of interest within the build. The microstructural simulation utilizes the time and temperature data for a unique position to track the evolution of microstructure based on the thermal excursions occurring at that location within the build. The output of the microstructural simulation is a text file describing phase constitution and microstructural features as a function of time and temperature, such as percentage of α and β formed in an α/β titanium alloy or precipitate size and number density within a precipitation strengthened nickel-based alloy. The description of the microstructure at the time defined as terminal is used within the mechanical property analysis to determine anticipated properties associated with a position of interest within the build.

3. Process models

Process simulations are of interest for acquiring detailed insight into the additive manufacturing processes. Although a complete representation of the process requires significant details in the area of interaction, there are also important aspects that require a global perspective. This is especially important

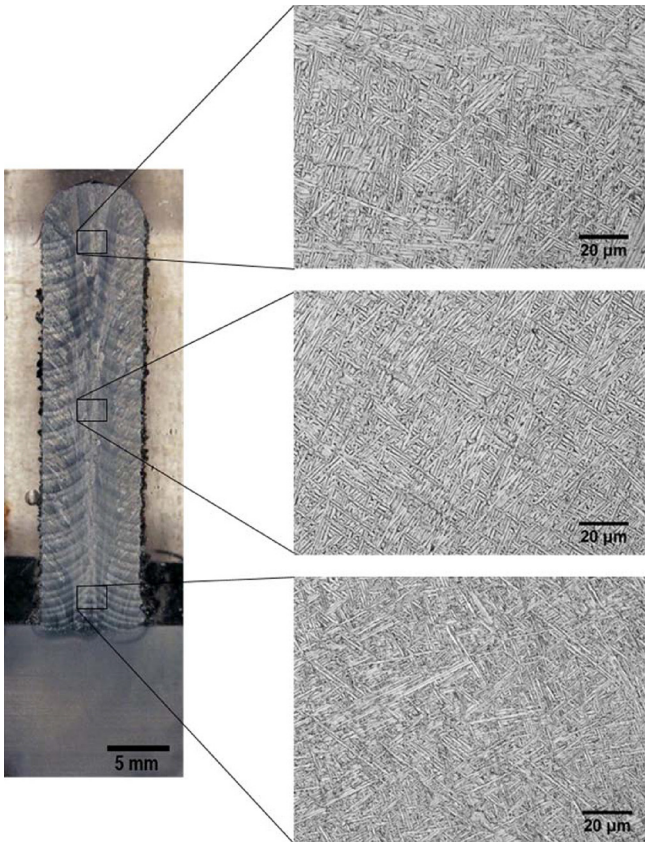

Fig. 4. Macrographic image (l) of a blade-type feature produced using directed laser deposition and Ti–6Al–4V powder along with micrographs (r) at three horizontal positions within the blade.

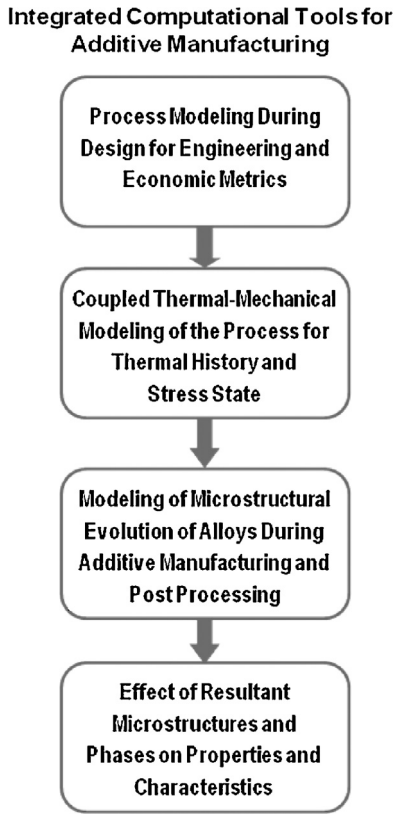

Fig. 5. Diagram showing integrated computational tools under development for describing various facets of additive manufacturing.

when examining the impact of the process on large, complex structures. Because the computational schemes that are required under these circumstances do not favor computational efficiency, two approaches are under development. One involves detailed modeling of the process under relatively simple geometries, while the other entails macro simulations of complex geometries. Both schemes have relevance depending upon the information that is desired, and the long term goal is the incorporation of both methods into a single model. It should also be noted that various features are incorporated into both models when appropriated.

Most additive manufacturing processes involve interaction of the heat source, a laser or electron beam, with the feedstock used for material addition and the substrate. A full description of these processes must include the amount of energy transferred from the heat source to the build layer, addition of material, conduction and convection of heat within the build layer and substrate, fluid flow within the liquid, and surface losses due to convention, radiation, and evaporation. The theoretical description of these transport phenomena involves the equations of conservation of mass, and momentum, and energy that have been used extensively for systems with moving heat sources, such as welding [11–15]. These governing equations are:

$$\text{for mass}: \quad \frac{\partial(\rho u_i)}{\partial x_i} = 0 \tag{1}$$

$$\text{for momentum}: \quad \frac{\partial(\rho u_j)}{\partial t} + \frac{\partial(\rho u_j u_i)}{\partial x_i} = \frac{\partial}{\partial x_i}\left(\mu \frac{\partial u_j}{\partial x_i}\right) - \rho U \frac{\partial u_i}{\partial x_i} + S_j \tag{2}$$

$$\text{and energy}: \quad \rho\frac{\partial(h)}{\partial t} + \frac{\partial(\rho u_i h)}{\partial x_i} = \frac{\partial}{\partial x_i}\left(\frac{k}{C_p}\frac{\partial h}{\partial x_i}\right) - \rho\frac{\partial \Delta H}{\partial t} - \partial\frac{\partial(u_i \Delta H)}{\partial x_i} + Q \tag{3}$$

solved by discretization and approximation of the solution using finite element or finite difference approaches. In the above equations, ρ is density, x is distance along three directions, u_i is velocity in the i-direction, t is time, k is thermal conductivity, C_p is specific heat, h is sensible heat, ΔH is latent heat content, μ is the effective viscosity, S_j represents the source term for momentum, and Q represents the energy source. The total enthalpy may be represented by the sum of the sensible heat and the latent heat. The application of latent heat is treated as a linear relationship between the liquidus and solidus temperatures of the material. Special consideration of the free surface within the computational domain is also necessary [16–18].

The energy provided to the substrate during directed energy deposition includes the energy provided by the laser or electron beam that is projected to the part, as well as the energy that is transferred to the substrate through the heated feed stock, which

is typically powder in the case of laser deposition and wire for electron beam processing. The total laser energy absorbed by the part may be defined by the bulk absorption coefficient, β:

$$\beta = 1 - \beta_p - \beta_S \tag{5}$$

where β_p is the amount of energy absorbed within the powder stream, and β_s is the amount of energy absorbed within the substrate. Although several factors influence the amount of energy that is absorbed, which include feedstock material, powder size, mass flow rate, power, and scan velocity, the bulk absorption coefficient may be measured directly and fairly accurately through calorimetry [19]. For directed energy processes, which generally are represented by a diffuse laser or electron beam, the model utilizes the bulk absorption coefficient obtained experimentally using a process calorimeter or estimates from data within the literature representing similar conditions. The total energy provide to the substrate, which is the product of the energy presented from the source and the bulk absorption coefficient, is distributed over an area based on the appropriate energy distribution, which is discussed below. Recent measurements for the total energy absorbed during directed laser deposition at 940 W of energy ($\lambda = 1.070$ nm) yielded a bulk absorption coefficient of 0.42 for Ti–6Al–4V alloy and 0.37 for Inconel 625™ [4].

The heat flux at the top surface, Q, may be defined through the use of a Fermi-Dirac function to approximate the top hat energy distribution for directed laser deposition [20]:

$$Q(r) = \frac{\beta q}{r^2}\left[1 + \exp\left(f\left(\frac{r}{R} - 1\right)\right)\right]^{-1} \tag{6}$$

where q is the power provided by the laser, r is the radius of the beam on the substrate, R is the beam waist, and f is a quality factor that aids in defining the sharpness of the top hat. It should be noted that because the distribution is asymptotic to the x-axis, the minimum spot size or beam waist (R) is defined when the intensity has fallen to some value. In many instances, the radius when the intensity has fallen to $1/e^2$ or approximately 13.5% of the peak intensity is used as the beam waist. Optical or probe devices may be used to measure the beam caustic, such as shown in Fig. 1, and are capable of calculating the beam waist. Detailed measurements of the spot size at varying distances from the focus optics, along with calculation of the beam divergence angle, may also be used to estimate the beam waist.

For powder bed fusion processes, the energy of the source is attenuated through the depth of the powder bed. Since energy is absorbed not only at the top surface but also through the depth, additional information that describes the scattering of the energy within the powder bed is necessary. This may also be measured but requires detailed experimentation to determine the attenuation factor that depicts the rate of absorption within the powder bed. A relationship has been developed that approximates the heat flux associated with laser irradiation representing a top hat distribution for the powder bed process [21]:

$$Q(r, z) = \left[\frac{\gamma}{1 - \exp(-\gamma t)}\right]\frac{\beta q}{\pi R^2}\exp(-\gamma z) \tag{7}$$

where z is the attenuation depth through the powder bed, t is the thickness of the powder bed, and γ is the attenuation coefficient.

In the case of large, complex geometries and associated paths of the heat source, the formulation is conducted within a rectilinear coordinate system (x, y, z) that moves with the heat source in the Lagrangian reference frame [22]. A transient conductive heat transfer analyses is performed to compute the temperature history which is then used as input to compute the resulting microstructure. Both temperature history and microstructure are the input to an elasto-plastic mechanical analysis to compute distortion and residual stress upon cooling. Deposition of material in additive manufacturing is modeled by using inactive or quiet elements which are activated as the added material (powder or wire) solidifies. Two methods are used for modeling material deposition: the use of quiet elements or the use of inactive elements [23–25]. In the quiet approach, the elements are present in the analysis but are assigned properties so they do not affect the analysis. In the inactive element approach, elements are not included in the analysis until the corresponding material has been added.

The amount of deposited metal in additive manufacturing may be significant, and as such, potential errors associated with modeling the metal deposition can be significant. As demonstrated in Ref. [18], accurate modeling of material deposition in additive manufacturing requires enforcing the discontinuity of the temperature field in the transition from active to inactive (or quiet) elements and tracing the continuously evolving surface of the deposited material to apply radiative and convective boundary conditions representing the process environment. Implementing both of these requirements in general purpose commercial FEA codes is either not feasible or computationally inefficient.

Building a complex part with additive manufacturing may require depositing hundreds or thousands of layers of material which introduces significant computational cost. Therefore, computational efficiency becomes paramount. To accelerate computing times, a new hybrid inactive/quiet element deposition method was developed by Michaleris [25] which is implemented in the physics based process model of the additive manufacturing FEA code CUBIC by Pan Computing LLC. In this approach, elements corresponding to deposition material are removed before processing. Then, elements are added layer by layer in a quiet state with properties that render them inactive. As the material is deposited, quiet elements are switched to active based on the location of the energy source. The hybrid inactive/quiet element activation approach maximizes computational performance by both reducing the active number of degrees of freedom and minimizing equation renumbering and solver initialization. Additional computational acceleration is achieved by octree H-adaptivity, as illustrated in Fig. 6. As new elements are added for each layer at the top of the build, elements are coarsened at previous layers such that the total number of degrees of freedom during the simulation is kept low even when modeling the deposition of very large parts. For example, Fig. 6(a and b) shows the temperature distribution during deposition of the 25th and 104th layer respectively. Elements are kept in a refined state near the active deposition layer and are coarsened for elements below. The approach results in significant improvement of

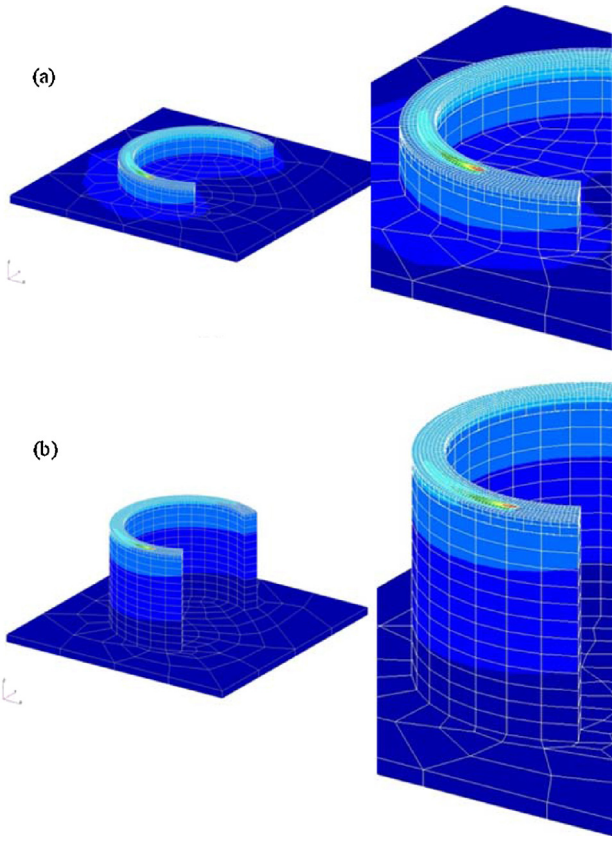

Fig. 6. Illustration of octree H-adaptivity in modeling additive manufacturing after (a) 25th layer and (b) 104th layer.

computational efficiency when compared to traditional FEA methods. The simulation shown in Fig. 4 was performed within 2.48 h on a 4 core 3.4 GHz i7 processor using octree H-adaptivity, while a traditional FEA approach required 176.27 h.

4. Material model

Two methods are being developed for predicting microstructural evolution during additive manufacturing. These techniques include DICTRA simulations for determining reaction kinetics of specific diffusional transformations and phase field modeling of spatial microstructural features during multiple transformations. Similar to the process modeling effort, both methods are being developed and employed depending upon the information that is desired, and they share common thermodynamics data developed by CALPHAD modeling. The materials models are highly material dependent, and the current focus during development has been on titanium and nickel-based alloys. The general approach for following microstructural transformations using these techniques are discussed briefly and details concerning these methods may be found within the references.

4.1. CALPHAD modeling of thermodynamics and atomic mobility and DICTRA simulations of phase transformations

The use of CALPHAD modeling enables important information for reactions of interest, such as transformation kinetics, to be applied to nonisothermal conditions found in additive manufacturing. The CALculation of PHAse Diagrams (CALPHAD) method is based on the idea that, if the Gibbs energy of every phase in a system is known as a function of temperature and composition, the phase fractions and compositions can be uniquely determined [26,27]. The goal, then, is to decompose the Gibbs energy into contributions that can be reused across different thermodynamic systems and extended into multi-component systems. A common decomposition for a phase is shown in Eq. (8).

$$G_{mf}^{phase}(T, P, N_i) = \Delta^{\circ}G_{mf} + \Delta^{id}G_{mf}^{mix} + \Delta^{xs}G_{mf} \tag{8}$$

The Gibbs energy per mole of formula of a phase, G_{mf}^{phase}, is the sum of (a) a weighted average of the Gibbs energy of the pure-component phases compared to a selected reference state, $\Delta^{\circ}G_{mf}$, (b) an ideal mixing contribution from configurational entropy, $\Delta^{id}G_{mf}^{mix}$, and (c) an excess contribution that captures all non-ideal interactions, $\Delta^{xs}G_{mf}$. The excess Gibbs energy includes differences in atomic bonding characteristics and other binary and ternary interactions between components. In practice, the formation energies and interaction parameters for the stable phases of many industrially relevant material systems have been developed in commercial and non-commercial databases, with new assessments published regularly in the literature. CALPHAD models are self-consistent and can be compared to experimental thermochemical data (e.g., calorimetry) as well as phase equilibria data (e.g., powder X-ray diffraction). As an example, the calculated isothermal section of the Ti–Al–V system at 700 °C and isopleth of Ti–6 wt%Al–V are shown in Fig. 7 using Thermo-Calc [28].

Consideration of the time-dependence of a phase transformation during the additive manufacturing process requires calculation of the diffusivities of all components as a function of temperature and composition. The CALPHAD approach can be applied to atomic mobilities for diffusion [28]. The diffusivity of substitutional species k in the composition gradient of species j in the lattice-fixed frame of reference, D_{jk}^{L}, is calculated within absolute reaction rate theory as follows.

$$M_i = M_i^{\circ} \exp\left(\frac{-\Delta Q_i}{RT}\right)\frac{1}{RT} \tag{9}$$

$$D_{kj}^{L} = \frac{M_k}{V_m}\frac{\partial \mu_k}{\partial \ln x_j} \tag{10}$$

where M_i and x_i are the atomic mobility and composition of species i, respectively, M_i° is a factor related to the frequency of atomic jumps between lattice sites, ΔQ_i is the activation energy for diffusion, V_m is the molar volume, and $\partial\mu_k/\partial x_j$ is the chemical potential gradient of species k with respect to species j. The CALPHAD modeling of M_i follows the similar procedure as Eq. (8) without the ideal mixing contribution term. As an example, the atomic mobilities of Al and V in the bcc phase are plotted in Fig. 8 as a function of V concentration [29].

With the thermodynamic and atomic mobility databases available, the diffusional phase transformations can be simulated using the finite difference code DICTRA [30], a program

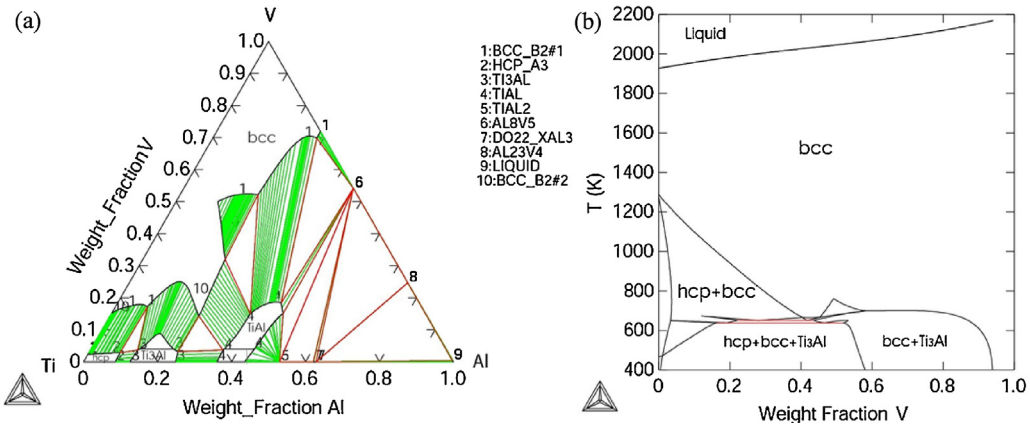

Fig. 7. (a) Calculated isothermal section at 700 °C; (b) calculated isopleth of Ti–6Al–V [23].

for simulating one-dimensional DIffusion-Controlled phase TRAnsformations (DICTRA) in multicomponent alloy systems. DICTRA is interfaced with Thermo-Calc, which handles all of the required thermodynamic calculations, e.g., thermodynamic factors for calculating interdiffusion coefficients, thermodynamic driving force for diffusion and phase transformation, and local equilibrium conditions at phase interfaces.

4.2. Phase field modeling

One of the main challenges in the highly nonisothermal conditions involved in additive manufacturing of metallic systems for complex geometries is to predict and control the local microstructures and properties. For example, a Ni-based superalloy or a Ti-alloy undergoes solidification and repetitive solid state phase transformations during repetitive thermal cycles, producing complex microstructures involving competitions among nucleation, growth, coarsening and compositional partitioning. It is difficult to fully characterize the microstructural evolution under different processing conditions through experiments since the experiments are generally not in situ and are only able to obtain a snapshot of a microstructure at the end of processing or after heat treatment.

One of the important roles that computational materials science can play in additive manufacturing is in modeling phase transformations and microstructural evolution for guiding development of a process for meeting predetermined material performance requirements. For example, a powerful microstructural modeling approach that has emerged over the last 10 years is the phase-field method [31–35] that has been applied to modeling microstructural evolution in a wide variety of materials processes ranging from solidification to microstructural coarsening and stress-induced morphological evolution. Hence, phase field simulation offer significant potential for describing microstructures obtained during additive manufacturing. Shown in Fig. 9 are microstructures obtained after directed laser deposition of Ti–6Al–4V alloy, along with microstructural simulations for a α/β alloy obtained under isothermal condition using the phase field approach [36]. Although in this example the results of the phase field models do not represent the thermal history associated with the deposition process, it does illustrate the potential of this method in simulating transformations associated with this alloy under the conditions found in additive manufacturing.

However, almost all existing phase-field models are formulated for isothermal conditions, and hence they need to be modified to handle non-isothermal conditions, e.g., multiple

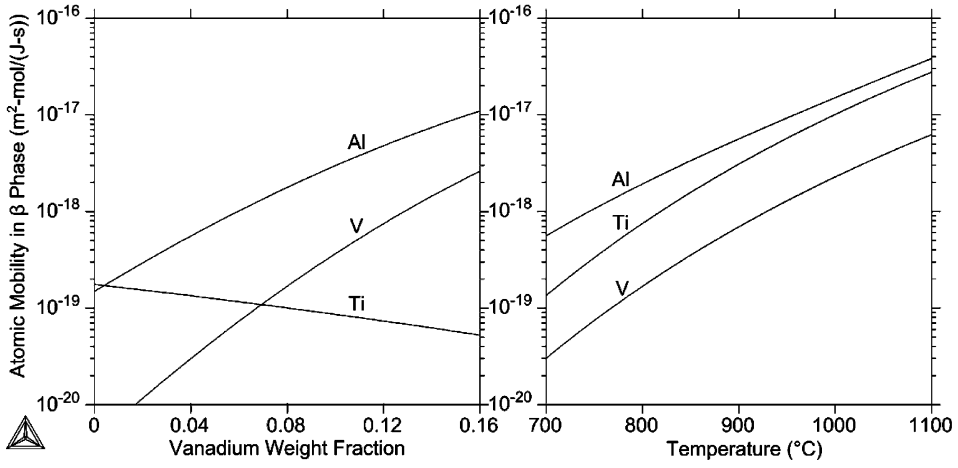

Fig. 8. Calculated atomic mobilities (a) in Ti–6Al–xV in β as a function of vanadium content at 700 °C, (b) in Ti–6Al–4V as a function of temperature.

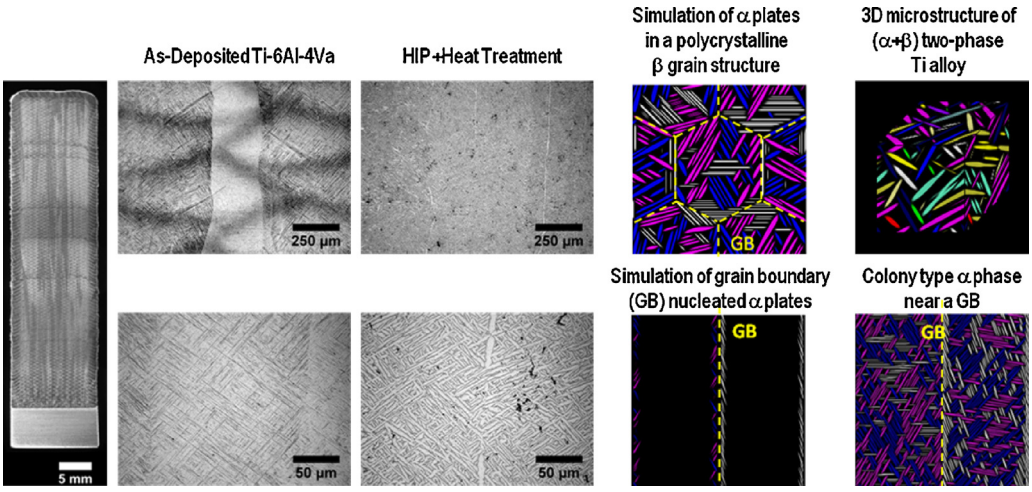

Fig. 9. Illustration of microstructures observed after additive manufacturing of Ti–6Al–4V alloy along with results of isothermal phase field simulations for an α/β titanium alloy.

thermal cycles, representative of additive manufacturing conditions [37]. It has also been recently shown that it is also possible to obtain effective properties of an arbitrary microstructure within the phase-field description. For example, the local effective modulus of a complex microstructure can be obtained by solving the elasticity equation taking into account the modulus variation in a microstructure [38]. This would allow the evaluation of local mechanical properties due to the spatial variation of temperature and composition. A much bigger challenge is to couple the phase-field model of microstructure evolution with crystal plasticity to obtain the local elastoplastic deformation [39]. Our preliminary effort along this direction shows that this is possible [40]. There is a need to build an efficient phase-field model integrating microstructural evolution and plasticity, which can be employed to determine both the plastic deformation of a microstructure and the microstructural evolution during additive manufacturing. Such microstructure and property modeling can be employed to produce quantitative information that can be validated with experimental measurements and characterization. It can also be used in conjunction with other thermo-mechanical based models to provide a tool for accelerating certification of components produced using additive manufacturing techniques.

5. Selected examples of simulations

5.1. Process simulations

Validation of the thermo-mechanical process model described above has been performed through experimental testing using in situ temperature and distortion measurements performed during electron beam deposition [41]. Initial application of the model is proving its utility for predicting and controlling residual stress and distortion of large parts of industrial scale produced using additive manufacturing techniques [42]. A Ti–6Al–4V plate approximately 380 cm long, 46 cm wide, and 25 mm thick was used as a substrate and several hundred kilograms of Ti–6Al–4V were deposited in 107 layers using the Sciaky VX-300 electron beam deposition system. The deposition path consisted of several thousand lines. The electron beam power was varied from 8 kW to 10 kW in order to control the melt pool size. Due to the size and complexity of the large part, a three stage modeling approach was implemented to simulate the entire deposition process. The first stage modeled the first layer of deposition, the second stage modeled the second through the ninth layers, and the third stage modeled all succeeding layers. The approach allowed for mesh coarsening between each stage, thus reducing the computational expense. Anti-symmetry was also used to model only half of the deposition. The analysis was performed using the code CUBIC by Pan Computing LLC.

Fig. 10 shows the computed final distortion for the part after it was released from the fixture. The figure includes both the modeled half portion and the other half which is plotted using anti-symmetry. 3D scan distortion measurements were obtained by Neomek Inc., as shown in the top view rendering in Fig. 11. A comparison between simulated and measured distortion along the edge of the part, as shown in Fig. 10, is displayed in Fig. 12. The simulated and experimental results are in good agreement.

5.2. Simulation of the diffusional phase transformation in Ti–6Al–4V alloy

The diffusional phase transformation for the $\beta \rightarrow \alpha + \beta$ reaction in Ti–6Al–4V was simulated by means of DICTRA for various cooling rates [22]. As mentioned above, the thermodynamic properties of both phases were modeled by means of the CALPHAD technique along with the atomic mobilities of Ti, Al, and V. Under the assumption of planar interface between the two phases and the local equilibrium condition at the phase interface, the diffusion fluxes and concentration profiles in both phases were updated at each time step, and the migration rate of the interface was then evaluated. The simulations are progressed with automatic adaptive grid spacing and

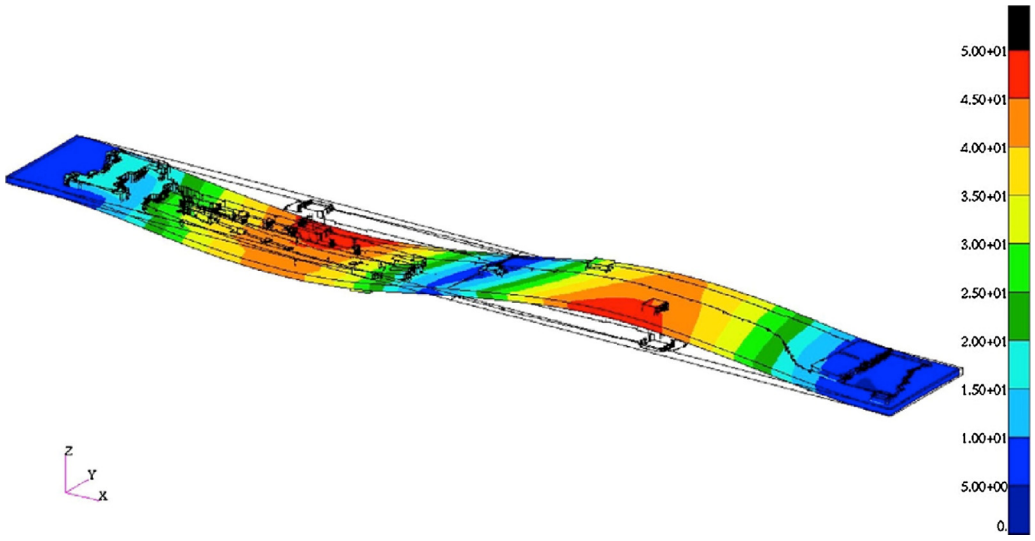

Fig. 10. Displacement magnitude in a large pard manufactured by the electron beam-based directed energy deposition process (mm, 2× magnification).

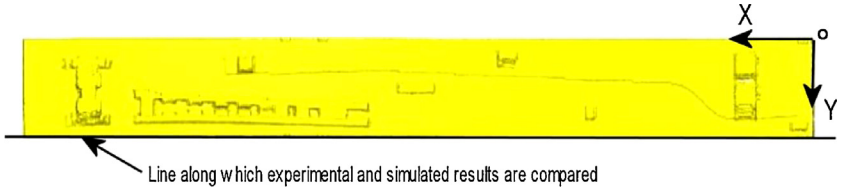

Fig. 11. Top view rendering of 3D scan of part, as provided by Nomek, Inc.

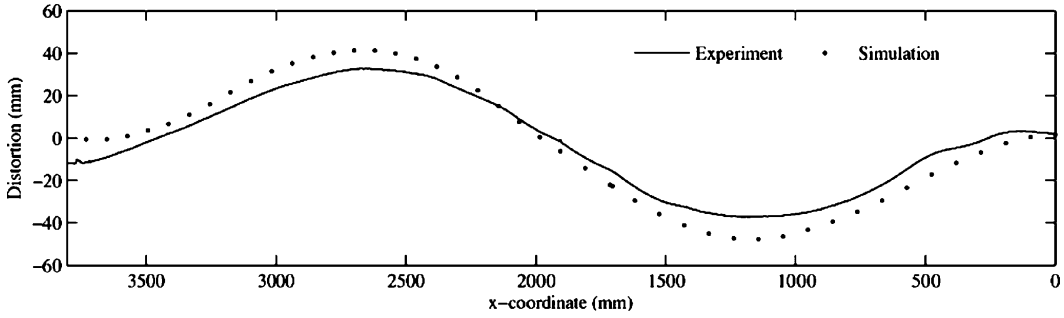

Fig. 12. Comparison of experimental and simulated distortion results in a large part manufactured by the electron beam-based directed energy deposition process.

adaptive time steps until reaching the pre-set simulation ending time.

The amount of the α phase formed during cooling from successive deposition passes was one important component in predicting mechanical properties for this alloy. Predictions for the amount of the α phase formed during three cooling rates are shown in Fig. 13. The equilibrium case is compared to two constant cooling rates. The thermodynamic model provides information about the system at equilibrium. However, the rapid heating and cooling cycles associated with the deposition process generally resulted in some deviation from equilibrium. By including composition- and temperature-dependent diffusivities in the model, the composition profile and motion of the α/β interface could be monitored as a function of simulated time.

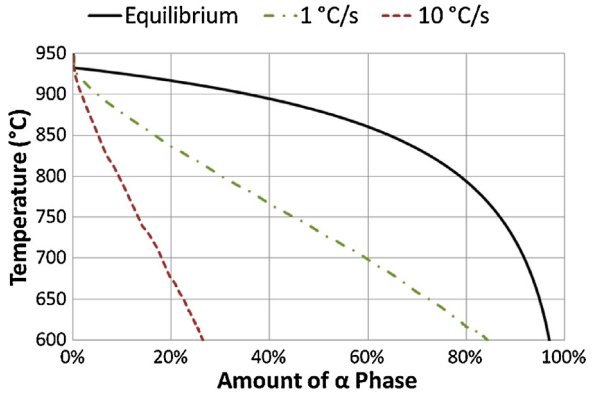

Fig. 13. Calculated phase fraction of α for a β-homogenized Ti–6Al–4V alloy during continuous cooling through diffusion-controlled simulations.

An implicit assumption for the simulation is that the phase transformation under consideration is diffusion-controlled. This assumption is not overly restrictive for directed laser deposition of titanium employing moderate heat input for producing larger components since the $\beta \rightarrow \alpha + \beta$ reaction will be controlled by solute diffusion for low cooling rates [43]. For high cooling rates, where large interface velocities drive the system to the martensitic regime, the fraction and composition of martensite can be estimated by performing the corresponding diffusion-controlled simulation at that cooling rate and assigning all retained β to martensite. The critical cooling rate delimiting these two regimes can be determined experimentally or by phase-field simulations.

6. Conclusions

The Center for Innovative Materials Processing through Direct Digital Deposition (CIMP-3D) at the Pennsylvania State University is developing an integrated computational system for describing important attributes of additive manufacturing of metallic components. The major computationally intensive components of this system include process models of the thermal and mechanical response of the material during processing and materials modeling to predict the development and evolution of microstructure during processing. The process models under development have the capability for simulating the two most common processes applicable to additive manufacturing of metallic materials: directed energy deposition and powder bed fusion. In both cases, the complexity of the part geometry and build path creates challenges for establishing and preserving an efficient computational mesh, and this is exasperated during simulation of large structures. An approach that is utilized for the computational scheme for global thermo-mechanical analysis of large structures is a hybrid inactive/quiet element activation technique that maximizes computational performance by both reducing the active number of degrees of freedom and minimizing equation renumbering and solver initialization. The materials models under development are primarily focused on titanium and nickel-based alloys. The minute scale associated with detailed microstructural analysis requires significant computational time; however, similar to the process modeling approach, two techniques are under development that may be used to optimize analysis based on the desired output. This includes CALPHAD modeling for determining reaction kinetics of specific diffusional transformations and phase field modeling of spatial microstructural features representing multiple transformations.

Acknowledgments

The authors would like to acknowledge the Open Manufacturing Program of the Defense Advance Research Project Agency for supporting portions of this work under ONR Grant N00014-12-1-0840 titled Manufacturing Demonstration Facility for Direct Digital Manufacturing (DDM). The authors would also like to acknowledge the contributions of Jamie Keist, Frederick Lia, Josh Park, Michael Gouge, and Josh Savitz in the preparation of this manuscript.

References

[1] Frazier WE. Metal additive manufacturing: a review. J Mater Eng Perform 2014;23:1917–28. ASM International.
[2] Blecher J, Palmer TA, Kelly SM, Martukanitz RP. Identifying performance differences in transmissive and reflective laser optics using beam diagnostic tools. Weld J Res Suppl 2012;91:204s–14s.
[3] Palmer T, Elmer J. Characterization of electron beams at different focus settings and work distances in multiple welders using the enhanced modified Faraday cup. Sci Technol Weld Join 2007;12:161–74.
[4] Lia F, Park J. Thermal response of metallic materials during additive manufacturing; 2014 [unpublished research].
[5] Zheng B, Zhou Y, Smugeresky JE, Schoenung JM, Lavernia EJ. Thermal behavior and microstructural evolution during laser deposition with laser-engineered net shaping: Part I, Numerical calculations. Metall Trans A 2008;39A:2228–36.
[6] Zheng B, Zhou Y, Smugeresky JE, Schoenung JM, Lavernia EJ. Thermal behavior and microstructural evolution during laser deposition with laser-engineered net shaping: Part II, Experimental investigation and discussion. Metall Trans A 2008;39A:2237–45.
[7] Reginster S, Mertens A, Paydas H, Tchuindjang J, Contrepois Q, Dormal T, et al. Processing of Ti alloys by additive manufacturing: a comparison of the microstructures obtained by laser cladding, selective laser melting and electron beam melting. Mater Sci Forum 2013;765:413–7.
[8] Niendorf T, Leuders S, Riemer A, Richard HA, Tröster T, Schwarze D. Communications: highly anisotropic steel processed by selective laser melting. Metall Mater Trans B 2013, http://dx.doi.org/10.1007/s11663-013-9875-z.
[9] Kinsella ME, Evans D. Technology transition through collaborative R&D, metals affordability initiative: a government-industry technical program. Defense AT&L; 2007. p. 12–5.
[10] Murr LE, Gaytan SM, Ramirez DA, Martinez E, Hernandez J, Amato KN, et al. Metal fabrication by additive manufacturing using laser and electron beam melting technologies. J Mater Sci Technol 2012;28:1–14.
[11] Hi J, Tsai H. Heat and mass transfer in gas metal arc welding, Part 1: The arc. Int J Heat Mass Transf 2006;50:833–46.
[12] Lindgren L-E. Computational welding mechanics. Thermomechanical and microstructural simulations. Cambridge, UK: Woodhead Publishing; 2007.
[13] Rai R, Palmer T, DebRoy T. Arc–laser interactions and heat transfer and fluid flow in hybrid welding. In: David S, DebRoy T, DuPont J, Koseki T, Smartt H, editors. Proceedings of the 8th International Conference on Trends in Welding Research. ASM International; 2009. p. 313–20.
[14] Michaleris P, editor. Minimization of welding distortion and buckling. Modeling and implementation. Cambridge, UK: Woodhead Publishing; 2011.
[15] Raghavan A, Wei H, Palmer T, DebRoy T. Heat transfer and fluid flow in additive manufacturing. J Laser Appl 2013;25:052006.
[16] Scardovelli R, Zaleski S. Direct numerical simulation of free-surface and interfacial flow. Annu Rev Fluid Mech 1999;31:567–603.
[17] Fan Z, Sparks T, Ruan J, Sparks T, Liou F. Numerical and analytical modeling of laser deposition with preheating. In: Proceedings of the International Manufacturing Science and Engineering Conference. ASME; 2007. p. 37–51.
[18] Naber A, Martukanitz R. A phase-field model for simulation of the laser cladding process using a discontinuous viscosity variable and its approximation by finite element method. In: Proceedings of the 23rd International Congress on Applications of Lasers & Electro-Optics, vol. 97. 2004. p. 536–9.
[19] Martukanitz R, Melnychuk R, Copley S. Dynamic absorption of a powder layer. In: Proceedings of the 23rd International Congress on Applications of Lasers & Electro-Optics, vol. 97. 2004. p. 1404–9.
[20] Stockham A, Smith J. Comparison between a super Gaussian and a true top hat. In: Forbes A, Lizotte T, editors. Laser beam shaping IX, vol. 7062. SPIE; 2008. p. 706201.
[21] McVay R, Melnychuk R, Todd J, Martukanitz R. Absorption of laser irradiation in a porous powder layer. J Laser Appl 2007;19:214–24.

[22] Kim C, Zhang W, Debroy T. Modeling of temperature field and solidified surface profile during gas-metal arc fillet welding. J Appl Phys 2003;94:2667–79.
[23] Lindgren L, Runnemalm H, Nasstrom M. Simulation of multipass welding of a thick plate. Int J Numer Methods Eng 1999;44:1301–16.
[24] Lindgren L, Michaleris P. Modeling of welding for residual stresses. In: Lu J, editor. Handbook on residual stress. SEM; 2005. p. 47–67.
[25] Michaleris P. Modeling heat transfer in additive manufacturing processes. Finite Elem Anal Des 2014;86:51–60.
[26] Kaufman L, Bernstein H. Computer calculation of phase diagrams with special reference to refractory metals, refractory materials, vol. 4. New York, USA: Academic Press; 1970.
[27] Liu Z-K. First-principles calculations and CALPHAD modeling of thermodynamics. J Phase Equilib Diffus 2009;30:517–34.
[28] Andersson JO, Helander T, Hoglund LH, Shi PF, Sundman B. THERMO-CALC & DICTRA, computational tools for materials science. CALPHAD 2002;26:273–312.
[29] Wang H, Warnken N, Reed RC. Thermodynamic and kinetic modeling of bcc phase in the Ti–Al–V ternary system. Mater Sci Eng A: Struct Mater Prop Microstruct Process 2010;528:622–30, http://dx.doi.org/10.1016/j.msea.2010.09.013.
[30] Liu Z-K, Chen L-Q. Applied computational materials modeling: theory, simulation and experiment. New York: Springer Science; 2007. p. 171–210.
[31] Boettinger W, Warren J, Beckermann C, Karma A. Phase-field simulation of solidification. Annu Rev Mater Res 2002;32:163.
[32] Chen L-Q. Phase-field models for microstructure evolution. Annu Rev Mater Res 2002;32:113.
[33] Moelans N, Blanpain B, Wollants P. An introduction to phase-field modeling of microstructure evolution. Comput Coupling Phase Diagr Thermochem 2008;32:268.
[34] Steinbach I. Phase-field models in materials science. Modell Simul Mater Sci Eng 2009:17.
[35] Provatas N, Elder K. Phase-field methods in materials science and engineering. Hoboken, USA: Wiley-VCH Verlag GmbH & Co. KGaA; 2010.
[36] Heo T [Ph.D. Dissertation] Phase-field modeling of microstructure evolution in elastically inhomogeneous polycrystalline materials. Pennsylvania State University; 2012.
[37] Martukanitz R, Howell P. Evolution of microstructure within the HAZ of precipitation strengthened aluminum alloys. In: Vitek J, David S, Johnson J, Smartt H, DebRoy T, editors. Proceedings of the 5th international conference on trends in welding research. ASM International; 1999. p. 227–32.
[38] Gaubert A, Le Bouar Y, Finel A. Coupling phase field and viscoplasticity to study rafting in Ni-based superalloys. Philos Mag 2010;90:375.
[39] Guo X, Shi S-Q, Ma X. Elastoplastic phase field model for microstructure evolution. Appl Phys Lett 2005;87:221910.
[40] Chen L, Chen J, Ji Y-Z, Heo T-W, Bhattacharrya S, Liu Z-K, et al. A fast Fourier transform based elasto-viscoplastic phase field model for 3D static recrystallization of polycrystal; 2014 [in press].
[41] Denlinger ER, Heigel JC, Michaleris P. Residual Stress and Distortion Modeling of Electron Beam Direct Manufacturing Ti–6Al–4V. J Eng Manuf 2014, http://dx.doi.org/10.1177/0954405414539494.
[42] Denlinger E, Irwin J, Michaleris P. Thermo-mechanical modeling of additive manufacturing large parts. J Manuf Sci Eng 2014 [unpublished research].
[43] Semiatin S, Knisley S, Fagin P, Barker D, Zhang F. Microstructure evolution during alpha–beta heat treatment of Ti–6Al–4V. Met Mater Trans A 2003;34:2377–86.